Trends in Chemistry

CellPress

Feature Review

Navigating CO utilization in tandem electrocatalysis of CO_2

Tianyu Zhang,[1] Zhengyuan Li,[1] Ashok Kumar Ummireddi,[1] and Jingjie Wu [1,*]

The transformation of CO_2-to-C_{2+} products on Cu catalysts suffers from limited C_{2+} selectivity and productivity due largely to sluggish C–C coupling kinetics. Sequential cascade CO_2-to-C_{2+} product conversion, integrating the first step CO_2-to-CO and second step CO-to-C_{2+} conversion in series on two distinct but complementary catalysts has been widely accepted as an effective approach to improve the *CO coverage that facilitates the C–C coupling rate. This review addresses the mechanism and design principles of tandem systems for CO_2 reduction, with a focus on tandem reduction in one electrolyzer. First, we analyze the crucial role of the adsorbed *CO in the C–C coupling process. Second, we thoroughly discuss the core design principle of the CO_2 tandem reduction systems: enhancing the CO utilization efficiency, navigated by improving CO intermediate transport, balancing the CO generation and utilization rate, and matching the CO generation and utilization overpotential between two independent catalysts. Third, we introduce the widely used technique to prepare the tandem catalysts and electrodes. Finally, we offer some perspectives on the outlook for CO_2 tandem reduction.

Highlights

Tandem CO_2 reduction, which integrates the cascade CO_2-to-CO and CO-to-C_{2+} product conversion in series on two distinct, complementary catalysts, provides an effective approach to circumvent the linear scaling relationship limitations and improve C_{2+} product generation.

The C–C coupling is the rate-determining step for generating C_{2+} products during electrochemical CO_2 conversion and the reaction rate is increased with the local CO concentration.

The design of tandem CO_2 reduction catalysts/electrodes should enable efficient CO transport, balance the CO generation and utilization rate, and match the CO generation and C_{2+} production overpotential.

Tandem catalysis as an effective strategy to achieve CO_2-to-C_2 product conversion

Electrochemical CO_2 reduction reaction (CO_2RR) into fuels and chemicals using renewable energy is an attractive technology that mitigates the massive amount of anthropogenic CO_2 emissions. Various catalysts have been discovered to convert CO_2 to specific value-added chemicals, such as CO on Ag, Au, and Zn [1–6] and HCOOH on Sn and Bi [7,8]. Among all screened metals, Cu stands out as a unique catalyst capable of yielding C_1/C_{2+} hydrocarbon and C_{2+} oxygenate products [9–11]. C_2H_4, as a typical C_{2+} product, is a key building block in the chemical industry to produce a wide range of plastics, solvents, and cosmetics, while C_2H_5OH is an essential liquid fuel for transportation. The huge global production capacity for C_2H_4 (201 Mt year^{-1} global production capacity) and C_2H_5OH (26 BG year^{-1} global production capacity) represents a promising match between market demand and the impactful mass of CO_2 reduction [12,13]. However, the CO_2-to-C_{2+} product conversion suffers from limited reaction selectivity and productivity, making this process less economically feasible. It has been widely accepted that the rate-determining step (RDS) for C_{2+} product formation is the C–C coupling between two adsorbed *CO, or *CO and its hydrogenation derivatives, of which the reaction rate and energy barrier are significantly affected by the local CO concentration (or *CO coverage) [14,15]. Improving C–C coupling reaction kinetics demands increased *CO coverage at the Cu surface to reduce the reaction activation energy [16], which underscores rational design of the electrochemical reaction system, including catalyst configuration, electrode structure, and electrolyzer arrangement.

High *CO coverage can be achieved by deconvoluting the CO_2-to-C_{2+} product conversion into two steps in series occurring on two distinct, complementary catalysts: CO_2-to-CO conversion on a CO-generation catalyst followed by CO-to-C_{2+} product conversion on a C_{2+}-generation catalyst (typically a Cu-based catalyst), which is so-called tandem CO_2RR [17,18]. Each step

[1]Department of Chemical and Environmental Engineering, University of Cincinnati, Cincinnati, OH 45221, USA

*Correspondence: wu2jj@ucmail.uc.edu (J. Wu).

can be optimized on its distinct catalyst. In the tandem CO_2RR process, the CO-generation catalyst provides supplementary CO to the Cu catalyst in addition to CO generated by Cu itself, improving the local CO concentration and subsequently *CO coverage of the Cu surface, while the Cu catalyst rapidly and continuously couples the CO to yield C_{2+} products. This tandem CO_2RR strategy enhances the *CO coverage on the Cu surface by introducing an *in situ* CO source instead of tuning the *CO binding energy on Cu and avoids the restriction imposed by the **linear scaling relations** (see Glossary) [9,19]. However, the success of tandem CO_2RR demands efficient CO utilization, for which gas (e.g., CO) transport is the main factor. The CO transport mode is largely governed by the spatial arrangement of the two complementary catalysts [20,21]. Moreover, the loading (or mass) ratio between two complementary catalysts and the compatible potential window for CO generation and coupling on the two different catalysts are also critical factors determining the CO utilization efficiency [22].

This review elucidates the central role of CO utilization in C–C coupling toward the selective and productive generation of C_{2+} products in the tandem CO_2RR, with a focus on the tandem reaction operated in one electrolyzer. The key aspects affecting CO utilization in the tandem CO_2RR are comprehensively discussed based on the experience we gained during CO_2 tandem reduction experimentation and knowledge acquired from the seminal works on this system. These factors include the CO transport from generation sites to utilization sites, the balance of CO generation and utilization rates, and the control of the reaction environment for both CO generation and utilization. An efficient tandem CO_2RR system adjusts the CO generation rate according to its demand on the Cu catalyst, delivers all the CO to the Cu surface for the successive C–C coupling reaction, and conducts CO generation and utilization with compatible environments. Following the design principle of the tandem CO_2RR system, the preparation strategies of tandem catalysts and electrodes are discussed. Finally, we provide insight into future research directions to improve the selectivity toward a specific C_{2+} product.

Why is CO so crucial for C_{2+} product generation?

CO as the key intermediate

The Cu catalyst can produce at least 16 different kinds of products from CO_2 electroreduction, including single-carbon products like CO, $HCOO^-$, and CH_4, multi-carbon products like C_2H_4, C_2H_5OH, CH_3COO^-, C_3H_7OH, and so on [23]. CO and $HCOO^-$ are produced at low overpotentials via a two-electron transfer pathway. A mixture of CH_4, C_2H_4, and multi-carbon liquid products is generated at more cathodic potentials (~ –0.60 to –1.20 V vs. RHE) [10,11,22,24–32]. The C_{2+} hydrocarbons or oxygenates start to evolve at a potential where the production rate of CO and $HCOO^-$ plateaus or decreases, indicating either CO or $HCOO^-$ is the key reaction intermediate [33]. However, experiments starting with HCOOH seldom show detectable products [34], and the hydrogenation of *OCHO to a deeper reduced intermediate *OCH_2O requires –1.9 V versus RHE according to the computational hydrogen electrode model, rendering this pathway thermodynamically unfeasible [35]. On the contrary, earlier experimental work found that the CO reduction shares a similar distribution of products as the CO_2 reduction on Cu [14,36–39]. Moreover, *in situ* Raman and Fourier transform-IR spectroscopies observed surface adsorbed *CO under CO_2 reduction [40–44]. Complementary to these experimental observations, the computational results demonstrate that the relationship between C_{2+} hydrocarbon productivity and the *CO adsorption energy on Cu is well aligned with the Sabatier principle [19,45]. All the evidence supports that the production of hydrocarbons and oxygenates proceeds through CO hydrogenation, whereas the HCOOH pathway is a dead end.

Reaction mechanism of C–C coupling

Identifying CO as the key intermediate significantly facilitates understanding the CO_2RR pathway and the C–C coupling mechanisms. The CO_2 reduction mechanism has been studied theoretically

Glossary

Eley-Rideal mechanism: describes a reaction between a reactant that has been chemisorbed and another one that has not been chemisorbed (i.e., directly from the gas or liquid phase).
Faradaic efficiency (FE): describes the ratio of electrons utilized for a specific electrochemical reaction to the total amount of electrons transferred.
Gas diffusion electrode (GDE): an electrically conductive substrate with a conjunction of a solid, liquid, and gaseous interface.
Langmuir-Hinshelwood mechanism: describes two molecules chemisorbed on neighboring sites; the adsorbed molecules undergo a bimolecular reaction.
Linear scaling relation: indicates that the stability of intermediates is linearly dependent on the binding energy of intermediates with the same adsorbing element or atom.
Proton concerted electron transfer (PCET) step: where e^- and H^+ move in a single chemical step.
Spillover: the transport of a species adsorbed or formed on a surface onto another surface.
Tandem CO_2 reduction: overall CO_2-to-C_{2+} product conversion reaction is performed via integrating the first step CO_2-to-CO conversion and second step CO-to-C_{2+} conversion in series on two distinct, complementary catalysts.

using either implicit solvent models that use approximations to treat the solvent as a continuum dielectric or explicit solvent models that depict solvent and ions at an atomistic level [13]. In general, the Gibbs free energies in the simulation may vary depending on the choice of solvent model. The consensus and discrepancies of CO_2 reduction mechanisms can be briefly summarized as follows. For the C_1 hydrocarbon pathway, the *CO is further reduced through either *CO➔*CHO or *CO➔*COH, depending on solvent models and Cu facets [46–48]. Regarding the C_2 pathway, the C–C coupling mechanism varies with different reaction conditions, including environment and catalyst configuration (Figure 1).

It is found that the Tafel slope (~118 mV dec^{-1}) of C_{2+} production is pH-independent, indicating that the RDS of C_{2+} product formation does not involve a **proton concerted electron transfer (PCET) step** [43]. The RDS of C_{2+} product formation is widely believed to be the C–C coupling [49,50]. However, the C_{2+} production rate at various pH values is affected by the competitive C_1 pathway (e.g., *CO➔*COH➔*CHOH) with intensive PCET [51]. C_{2+} production is suppressed at a low pH value and becomes more competitive at a high pH value.

The applied potential is a significant factor that affects the C–C coupling mechanism. At low overpotentials, the C–C coupling proceeds through the dimerization of two adsorbed *CO, whereas the coupling between CO and *CHO becomes more favorable at high overpotentials. Bell, Head-Gordon, and colleagues proposed that the *CO dimerization becomes kinetically unfavorable as the dipole–dipole repulsion between two *CO elevates with the increase of overpotential [48]. Instead, *CO couples with its hydrogenation derivatives such as *CHO more feasibly at high overpotentials.

The Cu catalyst configuration is another vital factor that intrinsically determines the C–C coupling mechanism. The d-band center of Cu catalysts varies upon differentiating facets, alloys, and morphologies, which affects the *CO adsorption strength, C–C coupling energy barrier, and the reaction pathway beyond the C–C coupling [52,53].

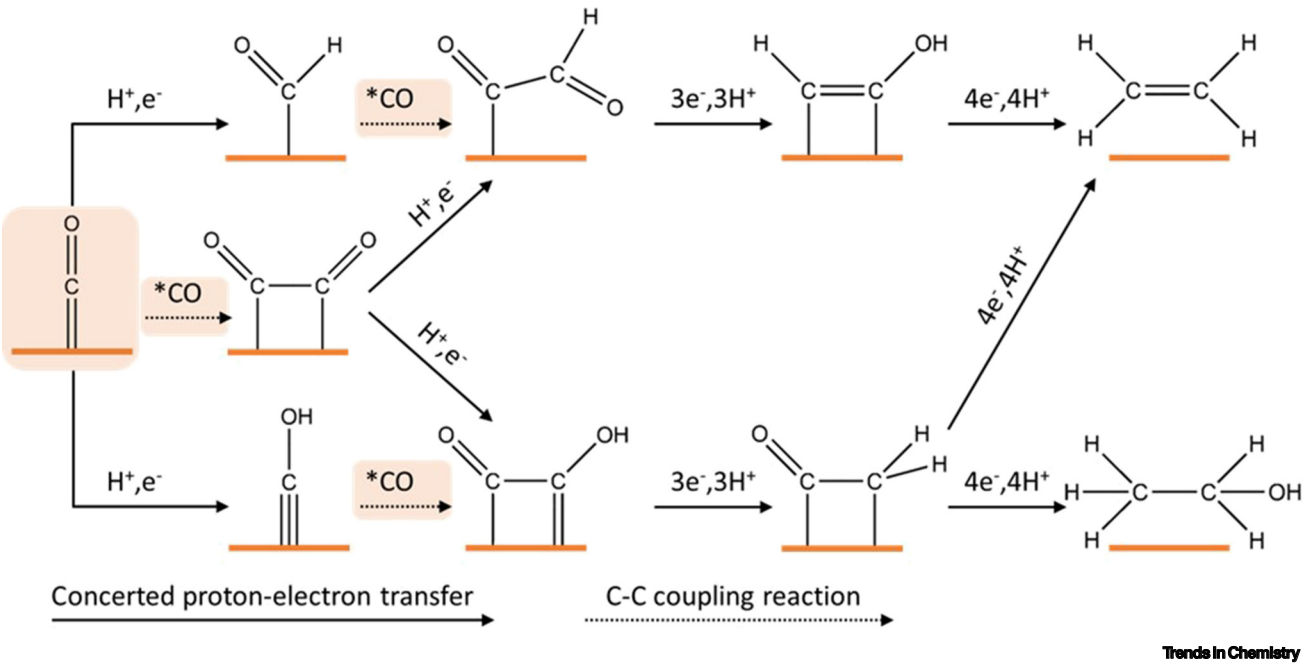

Figure 1. Representative proposed C–C coupling mechanism [13,102,103].

The electrolyte identity (cations and anions) is also involved in the C–C coupling step, although the mechanism remains elusive. Cations may promote C_{2+} product generation via forming a dense layer in the outer Helmholtz plane and creating a strong electric field [54,55]. The electric field assists in *CO stabilization and subsequently facilitates the C–C coupling. Anions influence the *CO adsorption strength via specific adsorption on the catalyst surface and the increase in *CO adsorption strength results in an increase in *CO coverage [56]. The aforementioned mechanisms underscore the significance of the *CO surface coverage in the C–C coupling rate and C_{2+} product selectivity.

Influence of *CO surface coverage on the C–C coupling rate

Since realizing the essence of CO intermediate during CO_2-to-C_{2+} product conversion, the **tandem CO_2 reduction** has evolved to promote the C–C coupling kinetics by increasing the local CO concentration and thereby increasing the *CO surface coverage on Cu. The *CO surface coverage governs the C–C coupling rate according to the following rate law [57]:

$$r_{C-C} = k\Theta_{*CO}^{\alpha} \quad [1]$$

where r_{C-C} is the C–C coupling reaction rate; Θ_{*CO} is the *CO surface coverage; α is the reaction order with respect to Θ_{*CO}; and k is the reaction rate constant determined by the Arrhenius equation.

It is noteworthy that the CO_2-to-C_{2+} product conversion follows a positive reaction order with respect to Θ_{*CO} [58]. Density functional theory computational results demonstrate that there is a second order dependence of C–C coupling on Θ_{*CO} over the Cu surface [58]. When CO_2RR is performed on **gas diffusion electrodes (GDE)**, the relationship of Θ_{*CO} versus partial pressure of CO (P_{CO}) resembles the Langmuir adsorption isotherm, which makes the C–C coupling less sensitive to P_{CO} change under high P_{CO} [14,59]. Therefore, the C–C coupling reaction order gradually decreases with the increase of P_{CO}. The heterogeneity of surface sites on Cu catalysts usually leads to a multicomponent Langmuir adsorption isotherm [60]. The step and kink sites adsorb CO stronger than terrace sites [61]. Nevertheless, the enhancement of Θ_{*CO} facilitates C–C coupling reaction kinetics according to the law of mass action [62].

To enhance the C–C coupling reaction rate, the CO_2-to-CO conversion rate should be promoted to enable a sufficient Θ_{*CO}. The *CO formation rate enhances with *CO binding energy. Additionally, it is a general trend that increasing *CO coverage lowers the activation energy barrier of C–C coupling, the extent of which varies with the Cu active sites and the C–C coupling mechanisms (e.g., CO–CO vs. CO–CHO) [16,31]. The Sabatier principle states that the *CO binding energy should be neither too strong nor too weak for a facile CO-to-C_{2+} product conversion. Moreover, according to the linear scaling relation, adjusting the *CO binding energy is not a simple task since the binding energy of intermediates with the same adsorbing element is linearly linked to one another [63]. Given this, the binding energy of *CO cannot be adjusted independently to other corresponding intermediates over a single catalyst. Hence, an innovative design paradigm, for example, tandem reaction, is demanded to circumvent the linear scaling relations.

How to design a tandem CO_2RR system?

Tandem CO_2 reduction divides the complex reaction pathway into two sequential steps: the CO_2-to-CO conversion on the CO-generation active sites and the subsequent CO-to-C_{2+} product conversion on the Cu-based sites so that the reaction activity of each distinct step can be tuned with high flexibility. Conceptually, feeding CO with an elevated P_{CO} to the Cu by tandem reaction promotes the production rate of C_{2+} products. However, the selectivity toward C_{2+}

products is governed by the utilization efficiency of CO that is generated on the CO-generation catalysts; failure to utilize this CO would result in high **Faradaic efficiency (FE)** of CO rather than C_{2+} products. Therefore, an efficient tandem CO_2RR system requires a rational design in mediating the CO transport between two active sites, balancing the generation and utilization rate of CO and matching the overpotential of two different active sites.

Efficient transport of CO intermediate

The commute of CO from the generation sites to the utilization sites is a prerequisite for enabling the cascade reaction. The concert of the cascade reaction depends on how efficiently CO transports. CO transport can be classified into three mechanisms: **spillover**, diffusion, and convection (Figure 2).

Spillover is extensively reported for *H transport in thermocatalysis [64,65]. The mechanism of *CO spillover across the boundary between the CO-generation catalyst and Cu in tandem CO_2 reduction remains elusive [65]. The spillover on the catalyst surface is restricted within a short nanometer-scale distance and requires two different catalysts located in close proximity. The common strategy is to design bimetallic nanomaterials with two segregated active sites, such as alloys [66–68], nanodimers [69], surface-decorated nanoparticles [18,41,70,71], core-shell structure [21,72], and layered nanomaterials [73,74]. For example, Cu–Au/Ag nano-frames exhibited three times C_2H_4 selectivity compared with Cu nanocubes (77% vs. 25%) [138]. The Ag-decorated Cu_2O nanowires demonstrated onefold improvement in j_{C2H4} at −1.05 V compared with Cu (Figure 3A–C) [41]. It should be noted that besides the tandem effect in the bimetallic materials, the strain or the internal charge flow in the boundary area also affects the activity of both catalysts [75].

Beyond the nanometer distance, the CO transport is dominated by diffusion, during which the CO first desorbs from the CO-generation catalyst surface into the bulk environment then re-adsorbs onto Cu sites [76]. Because there is a small fraction of CO-generation sites adjacent to Cu sites over the total CO-generation sites, the majority of the CO diffuses over a longer distance to be utilized [41]. Maximizing the utilization of desorbed CO for C–C coupling necessitates a rational design of the catalyst and electrode. The principle of the design is to maximize the CO residence time, which is the total time the CO spent in the catalyst layer (CL). At the catalyst level, introducing the nanocavities or core-shell structure can confine the CO intermediate to enhance the re-adsorption of CO to the Cu surface [21,72,77,78]. The Au@Cu_2O yolk-shell nanoparticle confines the CO within the porous structure, promoting the FE of C_2H_5OH above 50% [72]. The hierarchically porous Cu/Zn bimetallic catalyst also improves the CO residence time within the pores for deep reduction, achieving a C_2H_5OH FE of 42% [78]. The hierarchical structure possesses two types of pores at a macroscale of 320 nm and a mesoscale of 20 nm, respectively [78]. Hence, the electrochemically active surface area of the porous catalysts is 59-fold of the geometric surface area. The CO transport mechanisms involve diffusion and convection at the electrode level. Ager and coworkers created tandem plain electrodes with micropatterned Cu and Au lines on the SiO_2 wafer and found that CO diffusion is possible for the length up to 100 μm (Figure 3D–F) [76]. In their following work, the pyramid-textured Cu/Ag bimetallic plain electrode with the Cu and Ag plane folded with a high angle shortens the diffusion length of CO from Ag to Cu and the rougher surface may increase the CO residence time within the electrode (Figure 3G–I) [79]. This design improves the CO intermediates conversion to 80–90%. Convection can make the CO transport in effect for a longer distance of millimeter-scale and above. In a customized cell with a flowing electrolyte and plain electrodes, positioning the Ag catalyst upstream and Cu catalyst downstream increases the CO residence time. It illustrates a noticeable change of product distribution on the Cu catalyst [80]. The design of the tandem

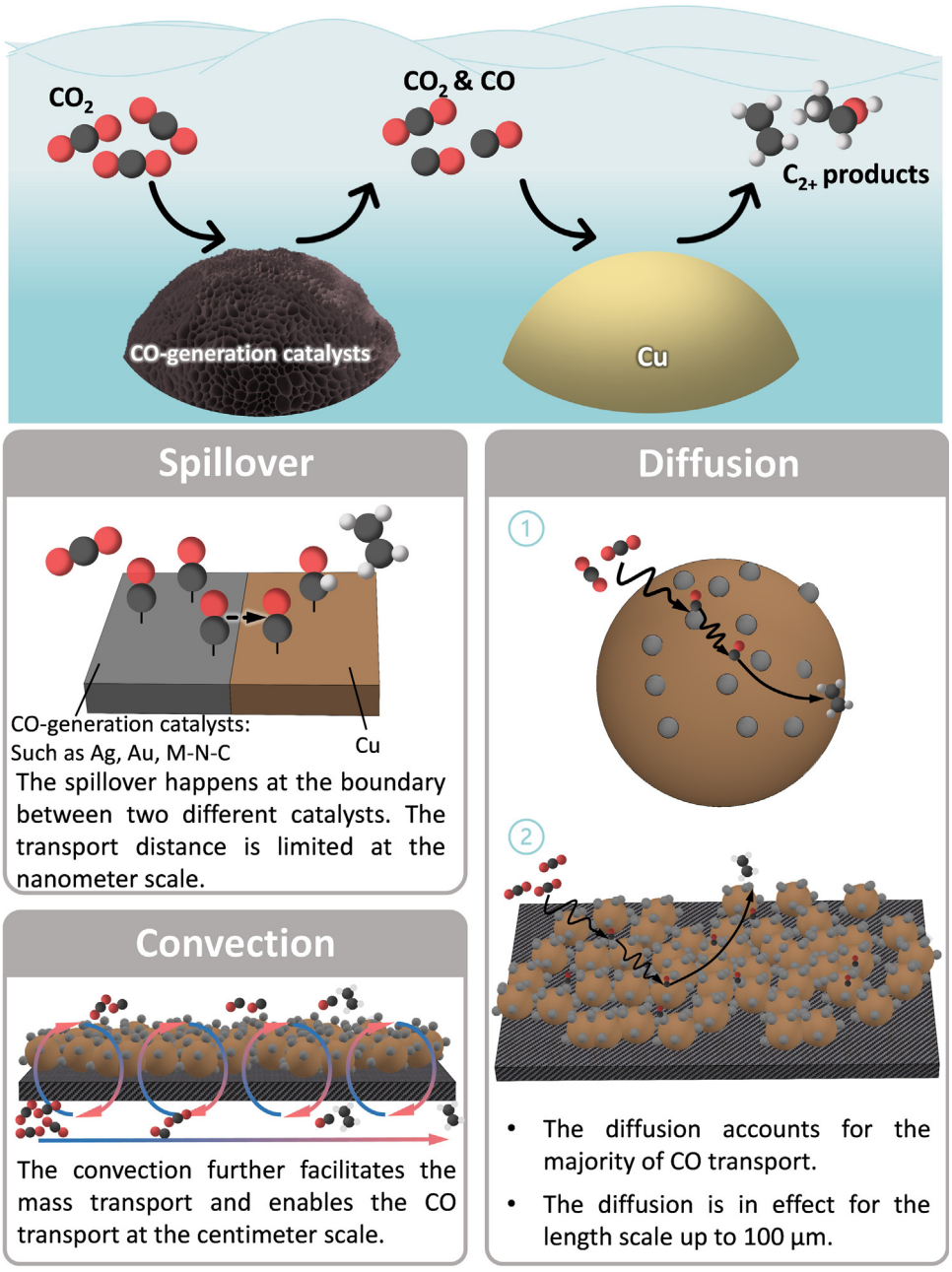

Figure 2. Schematic of the tandem CO_2 reduction process involving the CO intermediate and the three CO transport mechanisms.

plain electrodes focused on uniformly distributing the CO-generation catalyst onto the Cu catalyst and reducing the diffusion length. When the Cu catalyst is placed close to the CO source, the P_{CO} increases so that the CO conversion improves. However, the escape of CO into the bulk electrolyte strongly competes with the re-adsorption of CO onto the Cu surface, imposing a considerable limitation in increasing CO utilization. Moreover, it should be noted that, in the tandem plain electrodes, the fluxes of CO_2 and CO to the catalyst surface are low, resulting from the thick diffusion boundary

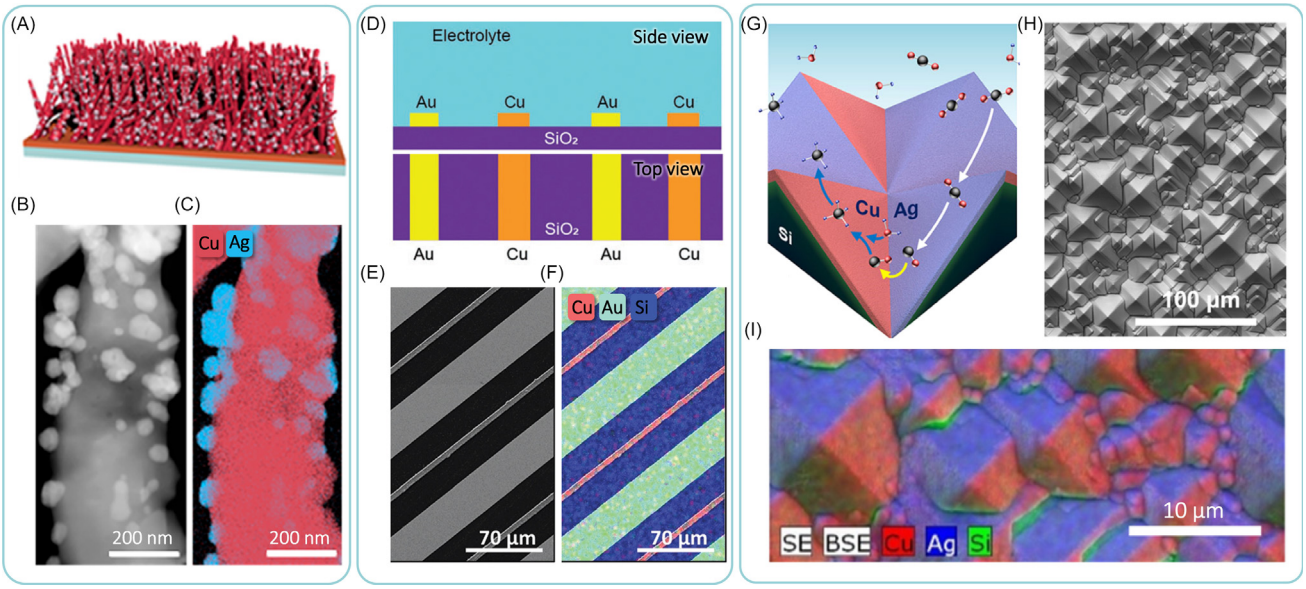

Figure 3. The representative design of tandem catalysts and electrodes involving CO spillover and diffusion. (A) Schematic, (B) transmission electron microscopy-high-angle annular dark-field image, and (C) respective scanning transmission electron microscopy-energy dispersive X-ray (EDX) mapping of Cu and Ag of the Ag-decorated Cu_2O nanowires [41]. (D) The side view (top) and top view (bottom) schematics, (E) scanning electron microscopy (SEM) image, and (F) EDX mapping of the interdigitated Cu/Au bimetallic plain electrode [76]. (G) The schematic, (H) the top view SEM image, and (I) EDX mapping of the pyramid-textured Cu/Ag bimetallic plain electrode [79].

layer (approximately 50 μm) [81]. The slow reactant transfer restricts the production rate in the tandem plain electrodes according to Equation 2, which limits its application in the industry [82].

$$j_L = nF\left(\frac{D}{\delta}\right)C_o \quad [2]$$

where j_L is the limiting current density, D is the gas diffusion coefficient (2.03×10^{-5} cm^2 s^{-1} for CO and 1.92×10^{-5} cm^2 s^{-1} for CO_2 at ambient conditions), C_O is the bulk concentration of gas reactant (32.95 mM for CO_2 and 0.99 mM for CO at 25°C and 1 atm), and δ is the diffusion layer.

For large-scale CO_2 reduction, a flow cell incorporating the GDE is used, allowing for significantly reduced diffusion boundary thickness down to the nanometer scale (double-phase boundary reaction) or direct gas phase CO_2 and CO reduction (triple-phase boundary reaction) [81,83]. Therefore, the C_{2+} production rate is improved by several orders of magnitude. The design of tandem electrodes based on GDE (denoted as tandem diffusion electrode) has a high possibility of being industrialized. In the tandem diffusion electrode, diffusion and convection at the electrode scale predominate in the CO transport mechanisms over spillover at the catalyst scale. A Cu/Ag tandem diffusion electrode composed of physically mixed Cu and Ag particles in the CL creates the CO-enriched gas environment. It improves the C_{2+} production rate by four times to –160 mA cm^{-2} compared with the bare Cu electrode (Figure 4A–C) [17]. The profile of local P_{CO} in the CL with a mixture of CO- and C_{2+}-generation catalysts is uniform but abruptly declines to the lowest, analogous to that in a continuous stirred tank reactor (CSTR), thus having a shorter CO residence time. Wu and colleagues first proposed the design of a layered tandem diffusion electrode inspired by the plug flow reactor (PFR) model, suggesting the significance of spatially managing the CO concentration distribution in the CLs to enhance the CO residence time [20,22,59]. In the PFR, the reactant (e.g., CO) is introduced at the inlet; therefore, the concentration tops at the inlet and gradually declines along the reactor length axis [20]. The CO residence time is maximized

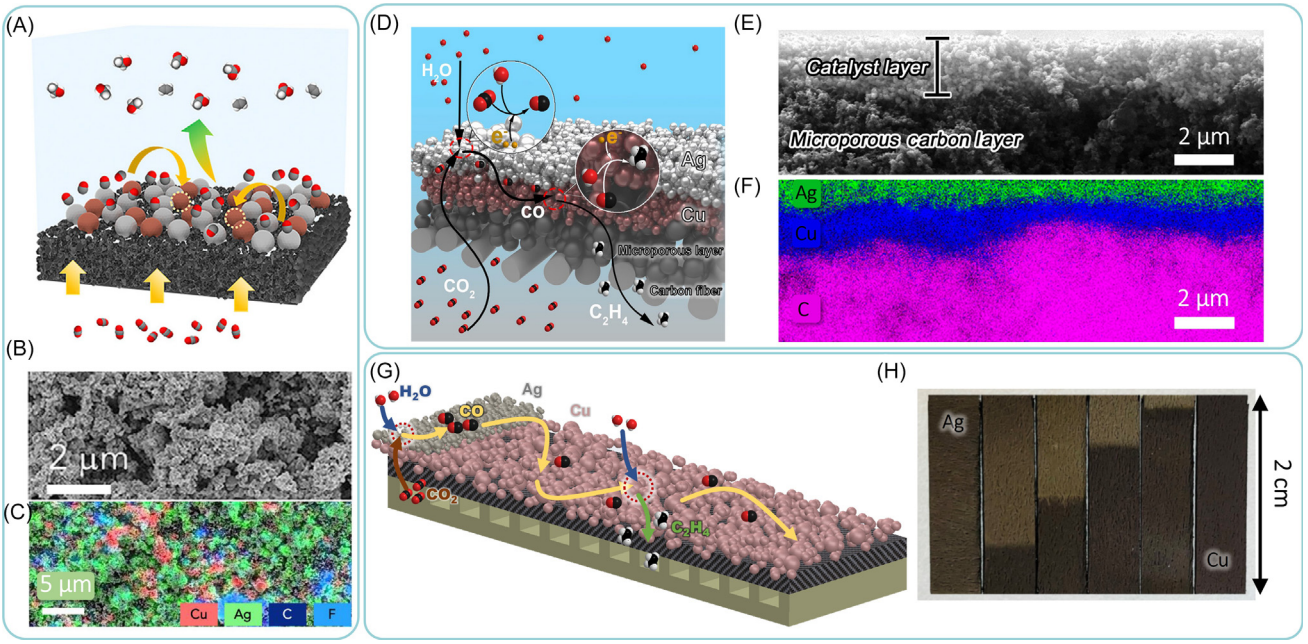

Figure 4. The representative design of tandem catalysts and electrodes involving CO diffusion and convection. (A) Schematic, (B) scanning electron microscopy (SEM) image, (C) and energy dispersive X-ray (EDX) mapping of the physically mixed Cu/Ag tandem diffusion electrode [17]. (D) Schematic, (E) SEM image, and (F) EDX mapping of Ag and Cu catalyst layers of the layered Cu/Ag tandem diffusion electrode [22]. (G) Schematic of the segmented Cu/Ag tandem diffusion electrode. (H) Photo of five representative Cu/Ag segmented tandem diffusion electrodes with different Cu/Ag area ratios and a bare Cu gas diffusion electrode [20].

in the PFR compared with that in the CSTR. In addition, since the C–C coupling reaction has a positive reaction order to CO, concentrating CO can further facilitate the CO-to-C_{2+} production conversion. The proposed layered tandem diffusion electrode consists of a thin layer of Ag CL on the top to generate a concentrated CO feed *in situ* and Cu CL underneath to couple the *in situ* generated CO (Figure 4D–F). During the tandem CO_2 reduction, the CO concentrates at the interface of Ag and Cu CLs and is rapidly converted to C_{2+} products as it diffuses back through the Cu CL. This layered architecture manipulates the CO concentration distribution along the thickness (micron scale) direction of CL and achieves C_{2+} FE of 87% at a j_{C2+} of –287 mA cm^{-2}. A segmented tandem diffusion electrode was designed to further increase the CO residence time, which comprises a segment of Ag CL at the inlet followed by a more extended segment of Cu CL downstream (Figure 4G,H). Such segment structure manages the CO concentration distribution in the electrode length direction at the centimeter scale at least. Convection plays a crucial role in transporting CO downstream. At the same time, CO diffuses back from the flow channel to the Cu CL for further reduction and coupling. Optimizing CO transport at the electrode scale shows a pronounced improvement in the C_{2+} FE of 90% at a j_{C2+} exceeding 1 A cm^{-2}.

Balance of CO generation and utilization rates

Another critical factor in improving the selectivity toward C_{2+} products in tandem CO_2 reduction is balancing the generation and utilization rates of the CO intermediate. Theoretically, the C_{2+} production rate on the Cu catalyst increases with P_{CO}, but that is not always the case for the C_{2+} selectivity in the tandem system [20,22,59]. During the tandem CO_2 reduction, we hope that the CO generated on the CO-generation catalyst can be converted entirely to C_{2+} products to achieve the best CO utilization. Hence, the FE of CO is minimized while the FE of C_{2+} products is maximized. Actually, the utilization of CO is restricted by the intrinsic activity of the catalyst, C–C

coupling rate law, and the tandem system design. First, the acceleration of the C_{2+} production rate is not linearly dependent on P_{CO} because the Θ_{*CO} levels off at the high P_{CO} region according to the Langmuir adsorption isotherm. Second, the CO molecules generated from the CO-generation catalyst will not transport to Cu with 100% efficiency as some CO molecules always escape from the CL prior to further conversion [22,80]. Furthermore, the energy barrier for C–C coupling on Cu is high, limiting the C–C coupling reaction rate [49]. If the CO utilization rate cannot compensate for the CO generation rate, a substantial quantity of uncoupled CO directly flows out of Cu CL. As a result, both the CO utilization efficiency and FE of C_{2+} products drop. Therefore, there must be a balance between CO generation and utilization rates.

In this regard, when the activity or loading of the CO-generation catalyst increases, the C–C coupling activity of Cu needs to be improved at a comparable pace. Various approaches, including defects, alloying, surface doping, crystal faceting, and subsurface oxygen engineering, have been developed to enhance the intrinsic activity of Cu catalysts [9,10,31]. For a defined tandem catalytic structure, including specific CO-generation and Cu catalysts, the balance between CO generation and utilization rates can be achieved by tuning the mass or surface area ratio between the CO-generation catalyst and Cu. Note that the CO-generation catalyst contributes a considerable portion of the CO supply but is not necessarily the primary CO source of C–C coupling since the Cu itself generates a higher amount of adsorbed *CO [20]. Even a tiny amount of extra CO (e.g., 1% by volume) added to the CO_2 feedstock can significantly improve the C_{2+} production rate [22]. Tuning the CO supply rate, in other words, the mass and surface area of CO-generation catalysts, is essential to amplify the FE of C_{2+} products. For instance, when fabricating the Cu/Ag layered tandem diffusion electrode containing commercial 25 nm Cu nanoparticles and 50 nm Ag nanoparticles, at a fixed loading of Cu nanoparticles, the C_{2+} production overpotential shifts anodically and the j_{C2+} under low overpotential region monotonically increases with the increase of Ag nanoparticles loading (Figure 5) [22]. However, the FE of C_{2+} products tops at a medium Ag loading (Figure 5) [22]. Oversupply of CO with higher Ag nanoparticles loadings decreases the CO utilization efficiency and thus deteriorates the selectivity toward C_{2+} products.

Synchrony of optimal reaction conditions for both active sites

To enable tandem CO_2RR, the electrolysis must be conducted in a condition where both the CO_2-to-CO and CO-to-C_{2+} product conversions are kinetically favorable. Thus, the optimal reaction

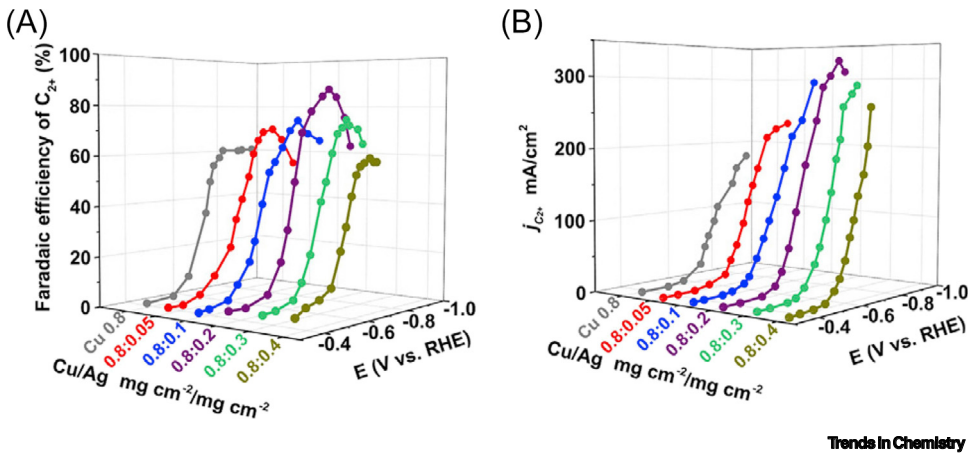

Figure 5. The importance of balancing CO generation and utilization rates. Dependence of (A) C_{2+} Faradaic efficiency and (B) C_{2+} partial current density on the Ag nanoparticles loading over Cu/Ag layered tandem diffusion electrode with a fixed Cu nanoparticle loading of 0.8 mg cm^{-2} but variable Ag nanoparticle loading from 0.05 to 0.4 mg cm^{-2}. Adapted, with permission, from [22].

conditions for both active sites should be synchronized. The electrocatalytic reaction of either CO_2-to-CO or CO-to-C_{2+} products is sensitive to the reaction conditions, like catalyst configuration, potential, CO partial pressure, local pH, and temperature [13,84]. The optimal condition for various reactions on distinct catalysts is generally different, especially the potential. The mismatch of the optimal reaction conditions sacrifices the catalytic activity of at least one of the catalysts. As shown in Figure 6A, the optimal potentials for C_{2+} products on Cu (–0.55 to –1.83 V vs. RHE) and CO generation on CO-generation catalyst (–0.40 to –1.14 V vs. RHE for Ag, Au, Zn, and single-atom catalyst) scatter in a large potential window and only partially overlap with each other. The C_{2+} generation requires relatively higher overpotentials than the CO production.

The most convenient way to solve the discrepancy of the optimal potential is by selecting two catalysts with significant overlapping. If direct overlapping is not possible for pristine catalysts, attempts should be made to modify the catalyst configuration and change the reaction environment to adjust the overpotential and even distinctively control the applied potential on the different catalysts if possible. First, the overpotential is intrinsically dictated by the adsorption energies of reactants and intermediates, as discussed earlier. The advanced catalysts still need to be rationally designed to reduce the C_{2+} product overpotential. The C–C coupling energy barrier is closely related to the electronic and geometric properties of catalyst surfaces. Second, CO_2 reduction is sensitive to the local environment. It has been widely studied that increasing the CO local concentration leads to a high *CO coverage, reducing the C–C coupling energy barrier and facilitating the reaction rate [16]. Studies using pure CO or mixed CO/CO_2 feedstock exhibit a decrease of overpotential for C_{2+} products in a magnitude of 0.2 V or even more (Figure 6B). Under the mixed CO/CO_2 feedstock, C–C cross-coupling between two reactive *CO stemming from CO_2 and CO, respectively, via the **Langmuir-Hinshelwood mechanism** will significantly enhance the C_{2+} production rate and reduce the C–C coupling overpotential [15]. Moreover, a high CO concentration in the outer Helmholtz layer favors the Eley-Rideal-type C–C coupling [85]. All the aforementioned evidence supports that the increased P_{CO} in the environment can facilitate the overlap of optimal reaction conditions on different catalysts by reducing the C_{2+} production overpotential. For example, a typical Au/Cu tandem catalyst shifts the alcohol generation overpotential positively by 90 mV more than the Cu catalyst. Under low overpotentials, the CO_2-to-high order product conversion rate on Au/Cu tandem catalysts is improved by over 100 times compared with the bare Cu catalyst [18]. In another example, the FeTPP[Cl]/Cu catalyst not only reduces the ethanol production onset potential by

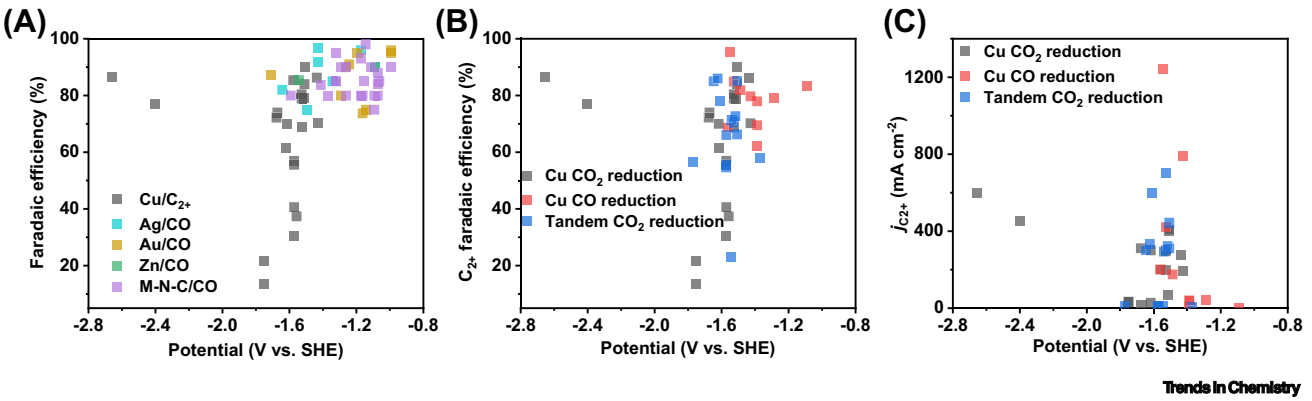

Figure 6. The synchrony of CO generation on CO-selective catalysts and CO utilization on Cu catalysts. (A) Comparison between the C_{2+} production potential on Cu [9–11,22,24–29,31,32,92,104,105] and the CO generation potential on Ag [1,4,106–111], Au [2,3,112–116], Zn [6,117], and single-atom catalysts (metal–nitrogen–carbon, M–N–C structure) [5,118–134]. The 3D cubes represent experimental results, while the 2D squares at the bottom represent the average potential for each kind of catalyst. (B,C) Summary of the partial current density of C_{2+}, Faradaic efficiency of C_{2+}, and corresponding applied potential for the direct CO_2 reduction reaction [10,11,22,24–32,92], CO reduction reaction [14,37,38,77,135–137], and tandem CO_2 reduction reaction [18,22,59,76,78,80,86] on Cu-based catalysts.

80 mV but also increases the ethanol FE by 12% compared with bare Cu catalyst [86]. Besides local CO concentration, it should be noted that the cations, anions, and pH value can also affect the reaction energy barrier, possibly via tuning the electric field in the double layer, specific adsorption onto the catalyst surface, and influencing the reaction pathway [36,56,58,60,87–89]. The detailed mechanistic roles for these factors are complex and, to date, poorly understood. Third, engineering the electrode or electrolyzer is also a feasible method to control the applied potential separately. A characteristic tandem electrode solves the discrepancy of overpotential by separating the CO-selective catalysts and Cu into two regions, thereby distinctly controlling the applied potentials [76,80]. This strategy demands two distinct anodes for the separate control of the cathode potential. Such a tandem electrode structure is more suitable for fundamental research while less applicable for industrial production. A tandem electrolyzer was proposed to conduct cascade CO_2 reaction in two electrolyzers in series, in which CO_2 is converted into CO at a high rate in the first electrolyzer and CO is further reduced in the second electrolyzer [90,91]. The tandem electrolyzer is convenient for separately controlling the reaction environment for the CO_2-to-CO conversion and CO-to-C_{2+} conversion in the terms of not only potential but also membrane, temperature, pH, and pressure. The tandem electrolyzer aims to utilize pure CO feedstock in the second electrolyzer to avoid CO_2 loss in the AEM electrolyzer. It is worth pointing out that the product selectivity depends on CO concentration. Pure CO reduction typically favors oxygenates (e.g., acetate) over hydrocarbon formation, resulting in downstream liquid separation issues.

How to prepare the tandem CO_2 reduction catalyst and electrode?

Tandem catalysts

The integration of multiple catalysts can be achieved by sequentially depositing each catalyst, including layer-by-layer deposition and seeded growth of different nanomaterials. Layer-by-layer deposition, typically physical vapor deposition and atomic layer deposition, allows precise control over layer thickness and surface structure [92,93]. For tandem catalysts involving a complex architecture such as core-shell structure, the gas accessibility toward the inner catalyst is challenging. Holes or slits need to be created on the outer catalyst by using either the sacrificial templates or densification/crystallization treatment on the outer catalyst [94,95]. Alternatively, applying photolithography during deposition to make a patterned electrode structure also enhances gas transport [76,79]. Physical deposition is a flexible method for various materials and more suitable for fundamental research.

Seeded growth using wet chemical processes can couple the two different catalysts in diverse structures [96]. This method is highly versatile since the synthesis condition can control the facet, morphology, and spatial distribution of the catalysts [97]. The most typical architectures include alloys, surface-decorated catalysts, metal nanodimers, and core-shell structures. However, it should be noted that the quality of the tandem catalysts is sensitive to the sophisticated synthesis conditions, such as the temperature, agitation, and even the reactor volume [97]. It imposes enormous difficulty in the scaling up of the catalyst production.

Tandem electrodes

The fabrication of tandem electrodes is more reproducible than tandem catalysts and easier to standardize because the factors that affect the electrode quality are relatively macroscopic and friendly to control [98]. Coating different catalysts onto different areas or segments of a gas diffusion layer (GDL) can fabricate the tandem GDE. Chemical and physical vapor deposition directly deposit metal nanoparticles or atoms onto the substrate [92,93]. Airbrush, screen printing, doctor blade, and slot-die use catalyst inks as media to coat the catalyst particles onto substrates. The CL properties, such as the gas permeability and ion conductivity, can be controlled by the ink composition, coating speed, and coating temperature [99].

The airbrush method is popular for preparing electrodes in both small and large sizes. It utilizes high-speed carrier gas and occasionally employs an ultrasonic nozzle to atomize the ink into micrometer-sized droplets for spraying [100]. Generally, the airbrush method provides compatibility with various substrates and minimizes catalyst wastage while spraying on large electrodes. These characteristics enable the convenient preparation of tandem GDEs with layered catalyst structures [22]. Moreover, when cooperating with masks or templates, the airbrush method is very flexible in producing tandem GDEs with segmented or patterned catalyst distribution [20]. However, the airbrush method suffers from coarse control over the CL thickness and porosity. Additionally, electrode preparation by the airbrush method is time-consuming. Screen printing, doctor blade, and slot-die are the widely used industrial-scale film deposition techniques satisfying the massive production capacity in the future [99,101]. These three techniques have better control over the layer thickness and porosity. The ink viscosity is crucial for these three techniques since it significantly affects the capillary action of ink to the substrates, CL thickness, and porosity. Besides ink viscosity, the CL thickness is determined by other factors, including the thickness and tension of the mesh in screen printing and the coating blade position in the doctor blade and slot-die. When all the parameters are fixed, the electrode can be produced continuously with persistent quality. Note that the doctor blade and slot-die can be integrated into a roll-to-roll system to continuously coat thin films on flexible substrates with the desired dimensions.

Concluding remarks

Tandem CO_2 reduction offers an alternative way to circumvent the limitation of linear scaling relations and facilitates the selectivity and productivity of C_{2+} products. The tandem CO_2 reduction has been performed at three levels: catalyst, electrode, and electrolyzer. However, at the catalyst scale, the spillover of CO across the boundary of different catalysts is still less understood (see Outstanding questions). Further, the C–C coupling mechanism may change with the increase of CO partial pressure coverage, which also demands further understanding. The cross-coupling of the *CO stemming from the adsorbed CO_2 and CO will account for a massive portion of the C–C coupling via the Langmuir-Hinshelwood mechanism. However, due to the increase of CO concentration in the outer Helmholtz plane, the dimerization of an adsorbed *CO and a free CO molecule from the electrolyte through the **Eley-Rideal mechanism** may contribute to the C–C coupling. The different C–C coupling mechanisms may eventually lead to different reaction selectivity, which needs more studies in the future.

The architecture of tandem GDEs also requires upgradation for more efficient CO transport. CO suffers from low solubility and sluggish transport in the electrolyte. The regular GDE is susceptible to flooding, resulting in a tortuous gas transport pathway and thicker diffusion layer. The ineffective CO transport reduces the CO concentration in the microenvironment and hampers the proceeding of tandem CO_2 reduction. The hydrophobicity or amphiphilicity of the CL and GDL should be further adjusted to facilitate CO transport. The flow field pattern needs further investigation to enhance gas diffusion and convection.

The current tandem CO_2 reduction has been focused on using CO as the intermediate for C–C coupling. However, the utilization of other candidates as intermediates, such as glyoxal (CHOCHO) and acetaldehyde (CH_3CHO), to improve the selectivity of post-C–C coupling toward a specific C_{2+} product, remains unexplored. Moreover, CH_3OH is an essential platform chemical feedstock, but its selectivity is low in current electrochemical systems. The tandem CO_2-to-CH_3OH conversion using an appropriate intermediate is worth an in-depth study.

Outstanding questions

At the catalyst scale, what is the CO spillover mechanism across the boundary between different active sites?

With the CO-generation catalysts as an additional CO source, how does the C–C coupling mechanism change with the increase of CO partial pressure or *CO coverage?

With the increase of CO local concentration, will the C–C coupling proceed through the Eley-Rideal mechanism between one adsorbed *CO and a free CO molecule?

The C–C coupling happens between different intermediates through the Langmuir-Hinshelwood or the Eley-Rideal mechanism. Will the reaction selectivity change by the different coupling mechanisms?

Both CO and CO_2 transport are restricted by their low solubility in water. The regular GDE is susceptible to flooding. How can the GDE architecture be restructured to mitigate the flooding so that the CO utilization efficiency can be further improved, enabling a long-term operation?

How do we design the gas flow pattern to facilitate gas diffusion and convection?

Given that the CO_2 reduction reaction has various intermediates, is there any intermediate other than CO that can be used as the tandem reaction intermediate?

Can tandem CO_2 reduction improve the productivity and selectivity of CO_2-to-CH_3OH conversion?

The tandem catalysis discussed here only focuses on one feedstock (e.g., CO_2). Can a similar tandem catalysis strategy be applied to multiple feedstocks to enable C–N, C–O bonding, or C–C coupling to form multiple carbon chemicals unachievable by CO_2 reduction only?

Acknowledgments

This work is supported by the National Science Foundation (Award No. CBET-2033343).

Declaration of interests

The authors declare no competing interests.

References

1. Kim, C. *et al.* (2015) Achieving selective and efficient electrocatalytic activity for CO_2 reduction using immobilized silver nanoparticles. *J. Am. Chem. Soc.* 137, 13844–13850
2. Zhu, W. *et al.* (2013) Monodisperse Au nanoparticles for selective electrocatalytic reduction of CO_2 to CO. *J. Am. Chem. Soc.* 135, 16833–16836
3. Rogers, C. *et al.* (2017) Synergistic enhancement of electrocatalytic CO_2 reduction with gold nanoparticles embedded in functional graphene nanoribbon composite electrodes. *J. Am. Chem. Soc.* 139, 4052–4061
4. Jee, M.S. *et al.* (2017) Stable surface oxygen on nanostructured silver for efficient CO_2 electroreduction. *Catal. Today* 288, 48–53
5. Huan, T.N. *et al.* (2017) Electrochemical reduction of CO_2 catalyzed by Fe-N-C materials: a structure–selectivity study. *ACS Catal.* 7, 1520–1525
6. Won, H.D. *et al.* (2016) Highly efficient, selective, and stable CO_2 electroreduction on a hexagonal Zn catalyst. *Angew. Chem. Int. Ed. Engl.* 55, 9297–9300
7. Han, N. *et al.* (2018) Ultrathin bismuth nanosheets from in situ topotactic transformation for selective electrocatalytic CO_2 reduction to formate. *Nat. Commun.* 9, 1320
8. Wu, J. *et al.* (2013) Electrochemical reduction of carbon dioxide: II. design, assembly, and performance of low temperature full electrochemical cells. *J. Electrochem. Soc.* 160, F953–F957
9. Zhong, M. *et al.* (2020) Accelerated discovery of CO_2 electrocatalysts using active machine learning. *Nature* 581, 178–183
10. De Gregorio, G.L. *et al.* (2020) Facet-dependent selectivity of Cu catalysts in electrochemical CO_2 reduction at commercially viable current densities. *ACS Catal.* 10, 4854–4862
11. Hoang, T.T.H. *et al.* (2018) Nanoporous copper-silver alloys by additive-controlled electrodeposition for the selective electroreduction of CO_2 to ethylene and ethanol. *J. Am. Chem. Soc.* 140, 5791–5797
12. Jouny, M. *et al.* (2018) A general techno-economic analysis of CO_2 electrolysis systems. *Ind. Eng. Chem. Res.* 57, 2165–2177
13. Nitopi, S. *et al.* (2019) Progress and perspectives of electrochemical CO_2 reduction on copper in aqueous electrolyte. *Chem. Rev.* 119, 7610–7672
14. Li, J. *et al.* (2019) Constraining CO coverage on copper promotes high-efficiency ethylene electroproduction. *Nat. Catal.* 2, 1124–1131
15. Wang, X. *et al.* (2019) Mechanistic reaction pathways of enhanced ethylene yields during electroreduction of CO_2–CO co-feeds on Cu and Cu-tandem electrocatalysts. *Nat. Nanotechnol.* 14, 1063–1070
16. Sandberg, R.B. *et al.* (2016) CO-CO coupling on Cu facets: coverage, strain and field effects. *Surf. Sci.* 654, 56–62
17. Chen, C. *et al.* (2020) Cu-Ag tandem catalysts for high-rate CO_2 electrolysis toward multicarbons. *Joule* 4, 1688–1699
18. Morales-Guio, C.G. *et al.* (2018) Improved CO_2 reduction activity towards C_{2+} alcohols on a tandem gold on copper electrocatalyst. *Nat. Catal.* 1, 764–771
19. Peterson, A.A. and Nørskov, J.K. (2012) Activity descriptors for CO_2 electroreduction to methane on transition-metal catalysts. *J. Phys. Chem. Lett.* 3, 251–258
20. Zhang, T. *et al.* (2022) Highly selective and productive reduction of carbon dioxide to multicarbon products via in situ CO management using segmented tandem electrodes. *Nat. Catal.* 5, 202–211
21. Monzó, J. *et al.* (2015) Enhanced electrocatalytic activity of Au@Cu core@shell nanoparticles towards CO2reduction. *J. Mater. Chem. A* 3, 23690–23698
22. She, X. *et al.* (2020) Tandem electrodes for carbon dioxide reduction into C_{2+} products at simultaneously high production efficiency and rate. *Cell Rep. Phys. Sci.* 1, 100051
23. Kuhl, K.P. *et al.* (2012) New insights into the electrochemical reduction of carbon dioxide on metallic copper surfaces. *Energy Environ. Sci.* 5, 7050–7059
24. Ma, S. *et al.* (2016) One-step electrosynthesis of ethylene and ethanol from CO_2 in an alkaline electrolyzer. *J. Power Sources* 301, 219–228
25. Wang, Y. *et al.* (2019) Catalyst synthesis under CO_2 electroreduction favours faceting and promotes renewable fuels electrosynthesis. *Nat. Catal.* 3, 98–106
26. Kibria, M.G. *et al.* (2018) A surface reconstruction route to high productivity and selectivity in CO_2 electroreduction toward C_{2+} hydrocarbons. *Adv. Mater.* 30, e1804867
27. Liang, Z.Q. *et al.* (2018) Copper-on-nitride enhances the stable electrosynthesis of multi-carbon products from CO_2. *Nat. Commun.* 9, 3828
28. Luo, M. *et al.* (2019) Hydroxide promotes carbon dioxide electroreduction to ethanol on copper via tuning of adsorbed hydrogen. *Nat. Commun.* 10, 5814
29. Li, Y. *et al.* (2020) Electrochemically scrambled nanocrystals are catalytically active for CO_2-to-multicarbons. *Proc. Natl. Acad. Sci. U. S. A.* 117, 9194–9201
30. Veenstra, F.L.P. *et al.* (2020) Laser-microstructured copper reveals selectivity patterns in the electrocatalytic reduction of CO_2. *Chem* 6, 1707–1722
31. Jiang, K. *et al.* (2020) Effects of surface roughness on the electrochemical reduction of CO_2 over Cu. *ACS Energy Lett.* 5, 1206–1214
32. Vasileff, A. *et al.* (2020) Electrochemical reduction of CO_2 to ethane through stabilization of an ethoxy intermediate. *Angew. Chem. Int. Ed. Engl.* 132, 19817–19821
33. Huang, Y. *et al.* (2017) Electrochemical reduction of CO_2 using copper single-crystal surfaces: effects of CO^* coverage on the selective formation of ethylene. *ACS Catal.* 7, 1749–1756
34. Cook, R.L. *et al.* (1989) Evidence for formaldehyde, formic acid, and acetaldehyde as possible intermediates during electrochemical carbon dioxide reduction at copper. *J. Electrochem. Soc.* 136, 1982
35. Peterson, A.A. *et al.* (2010) How copper catalyzes the electroreduction of carbon dioxide into hydrocarbon fuels. *Energy Environ. Sci.* 3, 1311–1315
36. Hori, Y. *et al.* (1997) Electrochemical reduction of CO at a copper electrode. *J. Phys. Chem. B* 101, 7075–7081
37. Jouny, M. *et al.* (2018) High-rate electroreduction of carbon monoxide to multi-carbon products. *Nat. Catal.* 1, 749–755
38. Wang, X. *et al.* (2019) Efficient upgrading of CO to C_3 fuel using asymmetric C-C coupling active sites. *Nat. Commun.* 10, 5186
39. Ozden, A. *et al.* (2021) Cascade CO_2 electroreduction enables efficient carbonate-free production of ethylene. *Joule* 5, 706–719
40. Chen, X. *et al.* (2020) Electrochemical CO_2-to-ethylene conversion on polyamine-incorporated Cu electrodes. *Nat. Catal.* 4, 20–27
41. Gao, J. *et al.* (2019) Selective C-C coupling in carbon dioxide electroreduction via efficient spillover of intermediates as supported by operando Raman spectroscopy. *J. Am. Chem. Soc.* 141, 18704–18714
42. Chang, X. *et al.* (2020) pH Dependence of Cu surface speciation in the electrochemical CO reduction reaction. *ACS Catal.* 10, 13737–13747
43. Li, J. *et al.* (2021) Electrokinetic and in situ spectroscopic investigations of CO electrochemical reduction on copper. *Nat. Commun.* 12, 3264
44. Malkani, A.S. *et al.* (2020) Cation effect on interfacial CO_2 concentration in the electrochemical CO_2 reduction reaction. *ACS Catal.* 10, 14871–14876
45. Liu, X. *et al.* (2017) Understanding trends in electrochemical carbon dioxide reduction rates. *Nat. Commun.* 8, 15438
46. Nie, X. *et al.* (2013) Selectivity of CO_2 reduction on copper electrodes: the role of the kinetics of elementary steps. *Angew. Chem. Int. Ed. Engl.* 52, 2459–2462
47. Shi, C. *et al.* (2016) Barriers of electrochemical CO_2 reduction on transition metals. *Org. Process. Res. Dev.* 20, 1424–1430
48. Garza, A.J. *et al.* (2018) Mechanism of CO_2 reduction at copper surfaces: pathways to C_2 Products. *ACS Catal.* 8, 1490–1499

49. Montoya, J.H. *et al.* (2013) Insights into C-C coupling in CO_2 electroreduction on copper electrodes. *ChemCatChem* 5, 737–742
50. Montoya, J.H. *et al.* (2015) Theoretical insights into a CO dimerization mechanism in CO_2 electroreduction. *J. Phys. Chem. Lett.* 6, 2032–2037
51. Xiao, H. *et al.* (2016) Mechanistic explanation of the pH dependence and onset potentials for hydrocarbon products from electrochemical reduction of CO on Cu (111). *J. Am. Chem. Soc.* 138, 483–486
52. Xin, H. *et al.* (2014) Effects of d-band shape on the surface reactivity of transition-metal alloys. *Phys. Rev. B* 89, 115114
53. Dickens, C.F. *et al.* (2019) An electronic structure descriptor for oxygen reactivity at metal and metal-oxide surfaces. *Surf. Sci.* 681, 122–129
54. Ringe, S. *et al.* (2019) Understanding cation effects in electrochemical CO_2 reduction. *Energy Environ. Sci.* 12, 3001–3014
55. Resasco, J. *et al.* (2017) Promoter effects of alkali metal cations on the electrochemical reduction of carbon dioxide. *J. Am. Chem. Soc.* 139, 11277–11287
56. Varela, A.S. *et al.* (2019) Tuning the catalytic activity and selectivity of Cu for CO_2 electroreduction in the presence of halides. *ACS Catal.* 6, 2136–2144
57. Bard, A.J. *et al.* (2022) *Electrochemical methods: Fundamentals and Applications*, John Wiley & Sons
58. Liu, X. *et al.* (2019) pH effects on the electrochemical reduction of CO_2 towards C_2 products on stepped copper. *Nat. Commun.* 10, 32
59. Zhang, T. *et al.* (2020) Enhance CO_2-to-C_{2+} products yield through spatial management of CO transport in Cu/ZnO tandem electrodes. *J. Catal.* 387, 163–169
60. Wang, L. *et al.* (2018) Electrochemical carbon monoxide reduction on polycrystalline copper: effects of potential, pressure, and pH on selectivity toward multicarbon and oxygenated products. *ACS Catal.* 8, 7445–7454
61. Rostrup-Nielsen, J. and Nørskov, J.K. (2007) Step sites in syngas catalysis. *Top. Catal.* 40, 23332692
62. Langmuir, I. (1922) Part II.—"Heterogeneous reactions". Chemical reactions on surfaces. *Trans. Faraday Soc.* 17, 607–620
63. Vojvodic, A. and Nørskov, J.K.J. (2015) New design paradigm for heterogeneous catalysts. *Natl. Sci. Rev.* 2, 140–143
64. Karim, W. *et al.* (2017) Catalyst support effects on hydrogen spillover. *Nature* 541, 68–71
65. Xiong, M. *et al.* (2021) Spillover in heterogeneous catalysis: new insights and opportunities. *ACS Catal.* 11, 3159–3172
66. Zhu, W. *et al.* (2019) Low-overpotential selective reduction of CO_2 to ethanol on electrodeposited Cu Au nanowire arrays. *J. Energy Chem.* 37, 176–182
67. Jia, F. *et al.* (2014) Enhanced selectivity for the electrochemical reduction of CO_2 to alcohols in aqueous solution with nanostructured Cu–Au alloy as catalyst. *J. Power Sources* 252, 85–89
68. Feng, Y. *et al.* (2018) Laser-prepared CuZn alloy catalyst for selective electrochemical reduction of CO_2 to ethylene. *Langmuir* 34, 13544–13549
69. Huang, J. *et al.* (2019) Structural sensitivities in bimetallic catalysts for electrochemical CO_2 reduction revealed by Ag–Cu nanodimers. *J. Am. Chem. Soc.* 141, 2490–2499
70. Herzog, A. *et al.* (2021) Operando investigation of Ag-decorated Cu_2O nanocube catalysts with enhanced CO_2 electroreduction toward liquid products. *Angew. Chem. Int. Ed. Engl.* 60, 7426–7435
71. Shen, S. *et al.* (2019) AuCu alloy nanoparticle embedded Cu submicrocone arrays for selective conversion of CO_2 to ethanol. *Small* 15, e1902229
72. Zhang, B.-B. *et al.* (2020) Tuning nanocavities of Au@Cu_2O yolk–shell nanoparticles for highly selective electroreduction of CO_2 to ethanol at low potential. *RSC Adv.* 10, 19192–19198
73. Ren, D. *et al.* (2019) Atomic layer deposition of ZnO on CuO enables selective and efficient electroreduction of carbon dioxide to liquid fuels. *Angew. Chem. Int. Ed.* 58, 15036–15040
74. Chang, Z. *et al.* (2017) The tunable and highly selective reduction products on Ag@Cu bimetallic catalysts toward CO_2 electrochemical reduction reaction. *J. Phys. Chem. C* 121, 11368–11379
75. Jansonius, R.P. *et al.* (2019) Strain engineering electrocatalysts for selective CO_2 reduction. *ACS Energy Lett.* 4, 980–986
76. Lum, Y. and Ager, J.W. (2018) Sequential catalysis controls selectivity in electrochemical CO_2 reduction on Cu. *Energy Environ. Sci.* 11, 2935–2944
77. Zhuang, T.-T. *et al.* (2018) Copper nanocavities confine intermediates for efficient electrosynthesis of C_3 alcohol fuels from carbon monoxide. *Nat. Catal.* 1, 946–951
78. Su, X. *et al.* (2020) Hierarchically porous Cu/Zn bimetallic catalysts for highly selective CO_2 electroreduction to liquid C_2 products. *Appl. Catal. B* 269, 118800
79. Liu, Y. *et al.* (2021) Tandem electrocatalytic CO_2 reduction with efficient intermediate conversion over pyramid-textured Cu-Ag catalysts. *ACS Appl. Mater. Interfaces* 13, 40513–40521
80. Gurudayal *et al.* (2019) Sequential cascade electrocatalytic conversion of carbon dioxide to C–C coupled products. *ACS Appl. Energy Mater.* 2, 4551–4559
81. Nguyen, T.N. and Dinh, C.T. (2020) Gas diffusion electrode design for electrochemical carbon dioxide reduction. *Chem. Soc. Rev.* 49, 7488–7504
82. Xing, Z. *et al.* (2021) Enhancing carbon dioxide gas-diffusion electrolysis by creating a hydrophobic catalyst microenvironment. *Nat. Commun.* 12, 136
83. Nesbitt, N.T. *et al.* (2020) Liquid–solid boundaries dominate activity of CO_2 reduction on gas-diffusion electrodes. *ACS Catal.* 10, 14093–14106
84. Xu, S. and Carter, E.A. (2019) Theoretical insights into heterogeneous (photo)electrochemical CO_2 reduction. *Chem. Rev.* 119, 6631–6669
85. Schreier, M. *et al.* (2018) Competition between H and CO for active sites governs copper-mediated electrosynthesis of hydrocarbon fuels. *Angew. Chem. Int. Ed. Engl.* 57, 10221–10225
86. Li, F. *et al.* (2019) Cooperative CO_2-to-ethanol conversion via enriched intermediates at molecule–metal catalyst interfaces. *Nat. Catal.* 3, 75–82
87. Monteiro, M.C.O. *et al.* (2021) Absence of CO_2 electroreduction on copper, gold and silver electrodes without metal cations in solution. *Nat. Catal.* 4, 654–662
88. Gao, D. *et al.* (2018) Activity and selectivity control in CO_2 electroreduction to multicarbon products over CuOx catalysts via electrolyte design. *ACS Catal.* 8, 10012–10020
89. Singh, M.R. *et al.* (2016) Hydrolysis of electrolyte cations enhances the electrochemical reduction of CO_2 over Ag and Cu. *J. Am. Chem. Soc.* 138, 13006–13012
90. Theaker, N. *et al.* (2018) Heterogeneously catalyzed two-step cascade electrochemical reduction of CO_2 to ethanol. *Electrochim. Acta* 274, 1–8
91. Jouny, M. *et al.* (2019) Carbon monoxide electroreduction as an emerging platform for carbon utilization. *Nat. Catal.* 2, 1062–1070
92. Dinh, C.-T. *et al.* (2018) CO_2 electroreduction to ethylene via hydroxide-mediated copper catalysis at an abrupt interface. *Science* 360, 783–787
93. Xie, C. *et al.* (2020) Surface and interface control in nanoparticle catalysis. *Chem. Rev.* 120, 1184–1249
94. Dasgupta, N.P. *et al.* (2013) Atomic layer deposition of platinum catalysts on nanowire surfaces for photoelectrochemical water reduction. *J. Am. Chem. Soc.* 135, 12932–12935
95. Yamada, Y. *et al.* (2011) Nanocrystal bilayer for tandem catalysis. *Nat. Chem.* 3, 372–376
96. Tan, C. *et al.* (2018) Epitaxial growth of hybrid nanostructures. *Nat. Rev. Mater.* 3, 1–13
97. Gawande, M.B. *et al.* (2016) Cu and Cu-based nanoparticles: synthesis and applications in catalysis. *Chem. Rev.* 116, 3722–3811
98. Mauger, S.A. *et al.* (2021) Development of high-performance roll-to-roll-coated gas-diffusion-electrode-based fuel cells. *J. Power Sources* 506, 230039
99. Park, I.-S. *et al.* (2010) Fabrication of catalyst-coated membrane-electrode assemblies by doctor blade method and their performance in fuel cells. *J. Power Sources* 195, 7078–7082
100. Jhong, H.R.M. *et al.* (2013) The effects of catalyst layer deposition methodology on electrode performance. *Adv. Energy Mater.* 3, 589–599
101. Stähler, M. *et al.* (2019) A completely slot die coated membrane electrode assembly. *Int. J. Hydrog. Energy* 44, 7053–7058

102. Cao, B. *et al.* (2022) Designing Cu-based tandem catalysts for CO_2 electroreduction based on mass transport of CO intermediate. *ACS Catal.* 12, 9735–9752
103. Birdja, Y.Y. *et al.* (2019) Advances and challenges in understanding the electrocatalytic conversion of carbon dioxide to fuels. *Nat. Energy* 4, 732–745
104. Zhou, Y. *et al.* (2018) Dopant-induced electron localization drives CO_2 reduction to C_2 hydrocarbons. *Nat. Chem.* 10, 974–980
105. Jung, H. *et al.* (2019) Electrochemical fragmentation of Cu_2O nanoparticles enhancing selective C-C coupling from CO_2 reduction reaction. *J. Am. Chem. Soc.* 141, 4624–4633
106. Delacourt, C. *et al.* (2008) Design of an electrochemical cell making syngas (CO + H_2) from CO_2 and H_2O reduction at room temperature. *J. Electrochem. Soc.* 155, B42–B49
107. Mistry, H. *et al.* (2017) Enhanced carbon dioxide electroreduction to carbon monoxide over defect-rich plasma-activated silver catalysts. *Angew. Chem. Int. Ed. Engl.* 56, 11394–11398
108. Lau, G.P. *et al.* (2016) New insights into the role of imidazolium-based promoters for the electroreduction of CO_2 on a silver electrode. *J. Am. Chem. Soc.* 138, 7820–7823
109. Liu, S. *et al.* (2018) Rational design of silver sulfide nanowires for efficient CO_2 electroreduction in ionic liquid. *ACS Catal.* 8, 1469–1475
110. Lu, Q. *et al.* (2014) A selective and efficient electrocatalyst for carbon dioxide reduction. *Nat. Commun.* 5, 3242
111. Liu, S. *et al.* (2017) Shape-dependent electrocatalytic reduction of CO_2 to CO on triangular silver nanoplates. *J. Am. Chem. Soc.* 139, 2160–2163
112. Marques Mota, F. *et al.* (2018) Toward an effective control of the H_2 to CO ratio of syngas through CO_2 electroreduction over immobilized gold nanoparticles on layered titanate nanosheets. *ACS Catal.* 8, 4364–4374
113. Zhao, S. *et al.* (2018) Influence of atomic-level morphology on catalysis: the case of sphere and rod-like gold nanoclusters for CO_2 electroreduction. *ACS Catal.* 8, 4996–5001
114. Saberi Safaei, T. *et al.* (2016) High-density nanosharp microstructures enable efficient CO_2 electroreduction. *Nano Lett.* 16, 7224–7228
115. Huan, T.N. *et al.* (2016) CO_2 reduction to CO in water: carbon nanotube–gold nanohybrid as a selective and efficient electrocatalyst. *ChemSusChem* 9, 2317–2320
116. Chen, Y. *et al.* (2012) Aqueous CO_2 reduction at very low overpotential on oxide-derived Au nanoparticles. *J. Am. Chem. Soc.* 134, 19969–19972
117. Wang, Y. *et al.* (2017) Zinc imidazolate metal-organic frameworks (ZIF-8) for electrochemical reduction of CO_2 to CO. *ChemPhysChem* 18, 3142–3147
118. Kumar, B. *et al.* (2013) Renewable and metal-free carbon nanofibre catalysts for carbon dioxide reduction. *Nat. Commun.* 4, 2819
119. Li, F. *et al.* (2017) Porous nitrogen–doped carbon derived from biomass for electrocatalytic reduction of CO_2 to CO. *Electrochim. Acta* 245, 561–568
120. Sharma, P.P. *et al.* (2015) Nitrogen-doped carbon nanotube arrays for high-efficiency electrochemical reduction of CO_2: on the understanding of defects, defect density, and selectivity. *Angew. Chem. Int. Ed. Engl.* 54, 13701–13705
121. Cheng, Y. *et al.* (2018) Atomically dispersed transition metals on carbon nanotubes with ultrahigh loading for selective electrochemical carbon dioxide reduction. *Adv. Mater.* 30, e1706287
122. Yang, H.B. *et al.* (2018) Atomically dispersed Ni(i) as the active site for electrochemical CO_2 reduction. *Nat. Energy* 3, 140–147
123. Ju, W. *et al.* (2017) Understanding activity and selectivity of metal-nitrogen-doped carbon catalysts for electrochemical reduction of CO_2. *Nat. Commun.* 8, 944
124. Varela, A.S. *et al.* (2015) Metal-doped nitrogenated carbon as an efficient catalyst for direct CO_2 electroreduction to CO and hydrocarbons. *Angew. Chem. Int. Ed. Engl.* 54, 10758–10762
125. Pan, F. *et al.* (2018) Identification of champion transition metals centers in metal and nitrogen-codoped carbon catalysts for CO_2 reduction. *Appl. Catal. B* 226, 463–472
126. Cui, X. *et al.* (2017) Selective etching of nitrogen-doped carbon by steam for enhanced electrochemical CO_2 reduction. *Adv. Energy Mater.* 7, 1701456
127. Wang, H. *et al.* (2016) Nitrogen-doped graphenes as efficient electrocatalysts for the selective reduction of carbon dioxide to formate in aqueous solution. *Green Chem.* 18, 3250–3256
128. Genovese, C. *et al.* (2018) Operando spectroscopy study of the carbon dioxide electro-reduction by iron species on nitrogen-doped carbon. *Nat. Commun.* 9, 935
129. Leonard, N. *et al.* (2018) The chemical identity, state and structure of catalytically active centers during the electrochemical CO_2 reduction on porous Fe-nitrogen-carbon (Fe-N-C) materials. *Chem. Sci.* 9, 5064–5073
130. Pan, F. *et al.* (2018) Unveiling active sites of CO_2 reduction on nitrogen-coordinated and atomically dispersed iron and cobalt catalysts. *ACS Catal.* 8, 3116–3122
131. Hu, X.-M. *et al.* (2018) Selective CO_2 reduction to CO in water using earth-abundant metal and nitrogen-doped carbon electrocatalysts. *ACS Catal.* 8, 6255–6264
132. Varela, A.S. *et al.* (2018) pH effects on the selectivity of the electrocatalytic CO_2 reduction on graphene-embedded Fe–N–C motifs: bridging concepts between molecular homogeneous and solid-state heterogeneous catalysis. *ACS Energy Lett.* 3, 812–817
133. Shi, J.-J. *et al.* (2018) Facile synthesis of iron and nitrogen doped porous carbon for selective CO_2 electroreduction. *ACS Appl. Nano Mater.* 1, 3608–3615
134. Wu, J. *et al.* (2015) Achieving highly efficient, selective, and stable CO_2 reduction on nitrogen-doped carbon nanotubes. *ACS Nano* 9, 5364–5371
135. Luc, W. *et al.* (2019) Two-dimensional copper nanosheets for electrochemical reduction of carbon monoxide to acetate. *Nat. Catal.* 2, 423–430
136. Wang, L. *et al.* (2019) Electrochemically converting carbon monoxide to liquid fuels by directing selectivity with electrode surface area. *Nat. Catal.* 2, 702–708
137. Pang, Y. *et al.* (2019) Efficient electrocatalytic conversion of carbon monoxide to propanol using fragmented copper. *Nat. Catal.* 2, 251–258
138. Xiong, L. *et al.* (2021) Breaking the linear scaling relationship by compositional and structural crafting of ternary Cu-Au/Ag nanoframes for electrocatalytic ethylene production. *Angew. Chem. Int. Ed. Engl.* 60, 2508–2518